

Time-resolved measurements of shock-induced cavitation bubbles in liquids

S. Koch · W. Garen · F. Hegedüs · W. Neu · R. Reuter · U. Teubner

Received: 19 October 2011 / Published online: 29 May 2012
© Springer-Verlag 2012

Abstract A novel experimental method for the measurement of cavitation bubble dynamics is presented. The method makes use of a collimated cw HeNe laser beam that is focused onto a photodiode. A cavitation bubble centered in the laser beam leads to refraction and thus changes the diode signal. With sufficient temporal resolution of the measurement, the evolution of the bubble dynamics, and in particular, the collapse, could be well resolved (limitation is only due to diode response and oscilloscope bandwidth). In the present work this is demonstrated with cavitation bubbles generated with high-power nanosecond and femtosecond laser pulses, respectively. Bubble evolution is studied in two different liquids (water and glycerine) and at different temperatures and pressures.

1 Introduction

Cavitation is a major source of erosion, for instance, of ship propellers, pumps and water turbines. In such systems, low pressure regions (pockets) exist where the water pressure suddenly becomes very low, almost a vacuum range.

These growing pockets, i.e. the “cavitation bubbles” propagate to high pressure regions, where they collapse spontaneously [1].

To investigate the cavitation phenomena experimentally, different methods of bubble generation are possible. One of them uses a powerful short laser pulse that is focused into a liquid generating an optical breakdown. During the successive plasma recombination, a fast growing and nearly spherical bubble arises. When the radius has reached its maximum, the bubble contracts continuously to a minimum and finally collapses with one or more rebounds. The onset and collapse of the bubble are usually combined with shock wave emission (laser-generated bubble and shock waves, LGBS). The life time of a cavitation bubble depends on the initial laser energy into the liquid breakdown and bubble formation usually in the order of a few microseconds up to several milliseconds. In the case of LGBS, referring to the shock waves, the time is much shorter, i.e. of the order of 10 ns to a few microseconds, respectively. Consequently, a corresponding temporal resolution although it is not easy to obtain would be required in LGBS experiments.

For experimental investigations on cavitation bubble dynamics, in general, there are two different methods, i.e., high-speed shadow photography with 10^4 – 10^8 frames/s [2, 3] and probe beam deflection (PBD) [4, 5]. With increasing distances from the plasma, these authors were able to obtain information on bubble dimension and wall velocities. A further method limited to very small bubbles is based on Mie scattering [6].

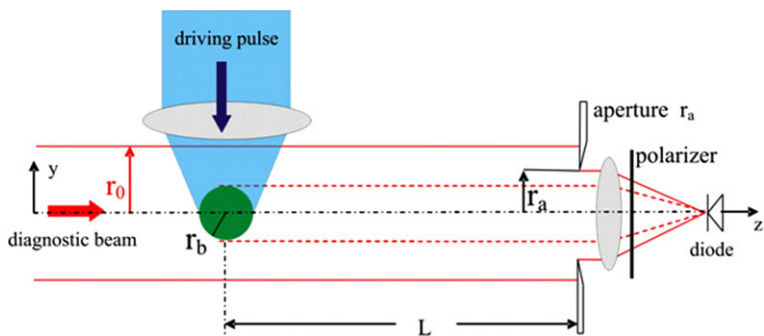
The present work reports on measurements of an alternative, novel and inexpensive optical method to enable a time-resolved insight into the formation and collapse of cavitation bubbles. Different energies, temperatures, and pressures have been studied in liquids with different viscosity (glycerine (propane-1,2,3-triol) and distilled water).

S. Koch (✉) · W. Garen · W. Neu · U. Teubner
Institut für Lasertechnik Ostfriesland, Hochschule Emden/Leer,
University of Applied Sciences, Constantiaplatz 4, 26723 Emden,
Germany
e-mail: sandra.koch@hs-emden-leer.de

F. Hegedüs
Department of Hydrodynamic Systems,
Budapest University of Technology and Economics, P.O. Box 91,
1521 Budapest, Hungary

R. Reuter · U. Teubner
Institute of Physics, Carl von Ossietzky Universität Oldenburg,
26111 Oldenburg, Germany

Fig. 1 Principle of measurement



The method provides also information on resulting shock waves from the initial state until the end of the rebound process. Under the assumption of a nearly spherical bubble, the method allows continuous measurements with temporal and spatial resolution of a complete cycle of bubble dynamics with a temporal resolution better than 20 ns depending on the sample rates of photodiode and oscilloscope. Contrary to Englert et al. [7], who studied luminescence of laser-induced bubbles by using a photomultiplier, a linear photodiode and a Gaussian diagnostic laser beam permit the calculation of the bubble radius in the present work.

2 Method of bubble diameter measurement

The principle of the method relies on laser beam deflection from a bubble that is centered on the axis of a HeNe laser beam of diameter r_0 (“diagnostic beam”, see Fig. 1). At a distance L behind the bubble, an aperture of radius r_a discriminates most of the deflected light. The undeflected part of the beam is collected and focused onto a photodiode. With respect to the signal in absence of a bubble, the measured signal is reduced by a polarizer and allows the bubble diameter to be deduced with temporal resolution. The temporal resolution is only limited by the readout system consisting of a fast photodiode and a fast oscilloscope. Laser beam deflection at the bubble could be simply estimated from geometrical optics (for details see Appendix A). Briefly, the parallel diagnostic beam hits the bubble of radius r_b , which is generated within a liquid by a further laser system (“driving pulse”) on the beam axis. The bubble is described as a homogeneous sphere of gas (or steam) with a refraction index (n_b) smaller than that of the ambient liquid (n_a).

Parallel rays of the diagnostic beam which propagate at $y > y_3$ (Fig. 9) from the optical axis are refracted by the bubble with a total deflection angle, ϵ , that depends on y coordinate and r_b . When y exceeds a certain value $y > r_b \cdot n_a/n_b$, total reflection occurs. In both cases, this results in divergent rays behind the bubble, which are mostly blocked by the aperture located far behind the bubble. Rays propagating $y \geq r_b$ are not affected and may still pass through the aperture where they will be detected.

To estimate the resulting “intensity” J of the diagnostic beam behind the aperture as a function of r_b , first an estimate of J in the absence of the bubble is made by integration of the diagnostic beam profile over the aperture area (Gaussian profile with $1/e^2$ diameter r_0 , and intensity on axis I_0 ; see Appendix A):

$$J_0 = \frac{\pi r_0^2 I_0}{2} [1 - e^{-2(\frac{r_a}{r_0})^2}] \tag{1}$$

If now, a bubble with a relative radius $\zeta = r_b/r_a$ is generated on axis of the diagnostic beam, ray deflection occurs. To deduce the bubble diameter, even for expanded bubbles, the following requirement must always be fulfilled: $r_0 > r_a > r_b$.

If one assumes that all deflected rays are blocked by the aperture (this is the case for $L \rightarrow \infty$), the detected intensity is reduced to

$$J(\zeta) = J_0 \left[1 - \frac{q - e^{-2(\frac{r_a}{r_0}\zeta)^2}}{1 - e^{-2(\frac{r_a}{r_0})^2}} \right] \tag{2}$$

(q is a correction which here is identical to 1). Due to the temporal evolution of the bubble size, ζ and hence $J(\zeta)$ depend on time t . When J is focused onto a diode with a linear response, from Eqs. (1) and (2) the bubble diameter could be deduced as a function of t (still $q \equiv 1$):

$$r_b(u(t)) = r_0 \sqrt{-\frac{1}{2} \ln[q - (1 - u(t)) [1 - e^{-2(\frac{r_a}{r_0})^2}]]} \tag{3}$$

where $u(t) = J(\zeta(t))/J_0$, i.e. the ratio of the photodiode signal with bubble at time t to the signal in absence of the bubble.

If the deflected rays are not totally blocked, the correction q in Eqs. (2) and (3) is no more identical to one, but becomes a function of $\zeta(u(t)) = r_b(u(t))/r_a$:

$$q(\zeta) = e^{-2[\frac{r_a}{2L(\frac{n_a}{n_b}-1)}\zeta]^2} \tag{4}$$

Hence, Eq. (3) becomes more complicate and has to be solved by iteration (the initial value of ζ and r_b , respectively, could be estimated from Eq. (3) (with $q = 1$); furthermore, for $r_a \ll L$ Eq. (4) may be linearized). However, as

may be seen from following sections, a correction is not always necessary. As an example, within the present work, $r_a = 2$ mm, $L \geq 500$ mm, $n_a = 1,33$, $n_b \approx 1$ (water and steam, respectively) and thus, for $\zeta \leq 1$ the deviation of q from 1 is smaller than 7×10^{-5} !

3 Experimental setup

Cavitation bubbles have been induced by two different laser systems into distilled water and glycerine, respectively (driving pulse in Fig. 1). The liquid has been kept in a quartz glass cuvette (volume = $3 \times 3 \times 3$ cm³) at a temperature $T = 25$ °C and a pressure $p = 1$ bar. Alternatively a stainless steel container (80 mm inner diameter and 200 mm height) is used to allow the temperature to be controlled in the range of 20 °C $< T < 100$ °C and the pressure to be kept between 0.2 bar $< p < 1$ bar (absolute values).

Two different laser systems have been used for inducing cavitation bubbles. A femtosecond laser was used for the experiment with different laser energies in water (laser fluence of max. 80 J/cm², pulse duration (FWHM) $\Delta\tau = 150$ fs,

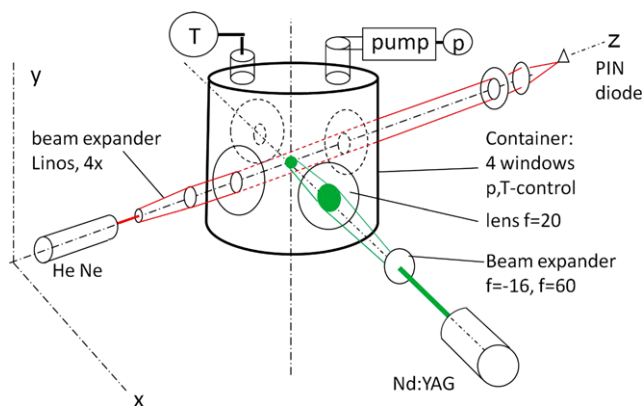


Fig. 2 Schematic sketch of the experimental setup

wavelength $\lambda = 775$ nm, CPA 2110 Ti:Sapphire, Clark-MXR, Inc.). A Q-switched Nd:YAG laser (laser fluence of 0.2 MJ/cm², $\Delta\tau = 6$ ns, $\lambda = 532$ nm, Solo III PIV 15, New Wave Research) was used for measuring glycerine and water, respectively, at different temperatures and pressures. The experimental setup using the container is shown in Fig. 2. Measurements with the femtosecond laser have been carried out by using the quartz glass cuvette.

An expanded, collimated diagnostic beam of a HeNe laser ($\lambda = 633$ nm, D-7517, Polytec) in TEM₀₀ mode crosses the bubble driving beam perpendicularly and is then detected by means of a PIN photodiode (BPW 34, Osram). The cavitation bubble generation is centered exactly in the middle of the diagnostic beam proved by a beam profiler (LBP-1, Newport). Figure 3 demonstrates the dip located in the maximum of the Gaussian beam.

The diagnostic beam (HeNe laser) is focused to the PIN diode, covered with a 633 nm interference filter (Schott, 10 nm band width) to discriminate environmental light. An oscilloscope (TDS7154B, Tektronix) is used to read out the voltage $U(t)$. A polarizer allows the intensity of the diagnostic beam to be adjusted. Part of the beam is blocked by the cavitation bubble. Thus, the temporal evolution of the diode voltage $U(t)$ depends on the temporal evolution of the bubble volume $V(t)$. Then, under the assumption of a spherical bubble geometry, the radius $r_b(t)$ of the bubble can be calculated as described earlier (Sect. 2). The assumption of the spherical bubble geometry is verified by a separate series of CCD images (SensiCam, PCO, fitted on a microscope) during the measurements (see Fig. 4, Table 1). This is only valid within the first bubble before the collapse. During the first rebound, the spherical condition for the shape of the shadow area (two-dimensional) is not fulfilled as shown in Fig. 4 ($\Delta t = 190$ μ s). However, the measurement from the image of the non-spherical area leads to an “equivalent-spherical” area of nearly the same bubble dimension estimated by the novel measurement method presented in this paper (Table 1).

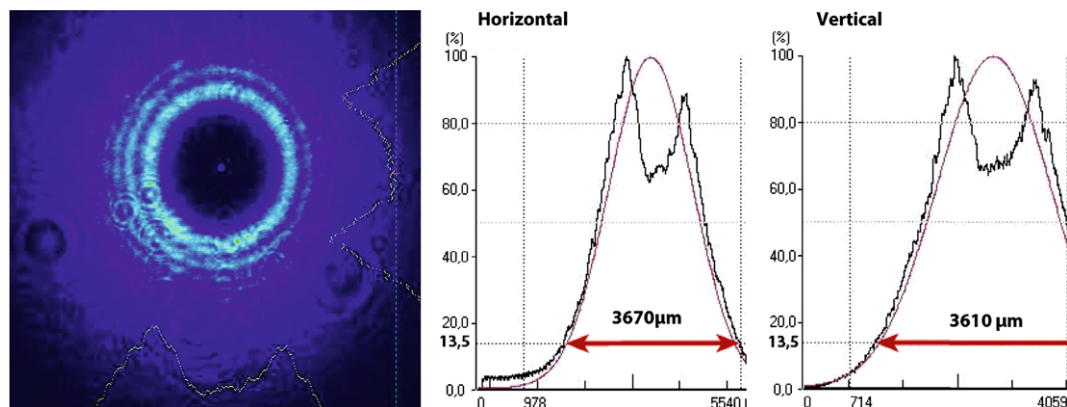


Fig. 3 Image in false color of the HeNe laser beam profile to verify the alignment of the cavitation bubble in the middle of the Gaussian beam

4 Results and discussion

The aperture of the experimental setup (Fig. 1) acts like a ‘schlieren device’, if strong gradients occur. It is a very sensitive possibility to detect initial and collapse shock waves as well as the time-depending bubble formation which can be seen in Fig. 5.

Figure 5a shows the bubble radius $r_b(t)$ for different laser energies induced by a femtosecond laser. The advantage of this method can be clearly seen in Fig. 5b. Beside the radius distribution $r_b(t)$, also the onset and collapse of the bubble are detectable (insert A and B). A temporal resolution of

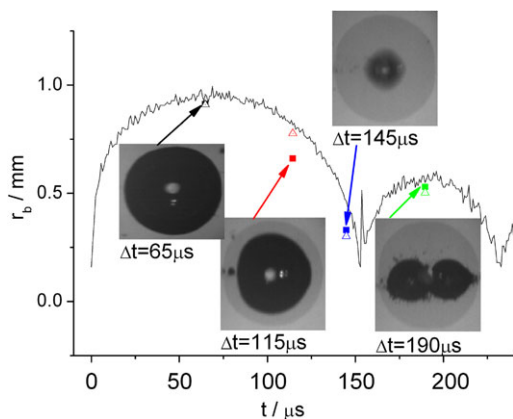
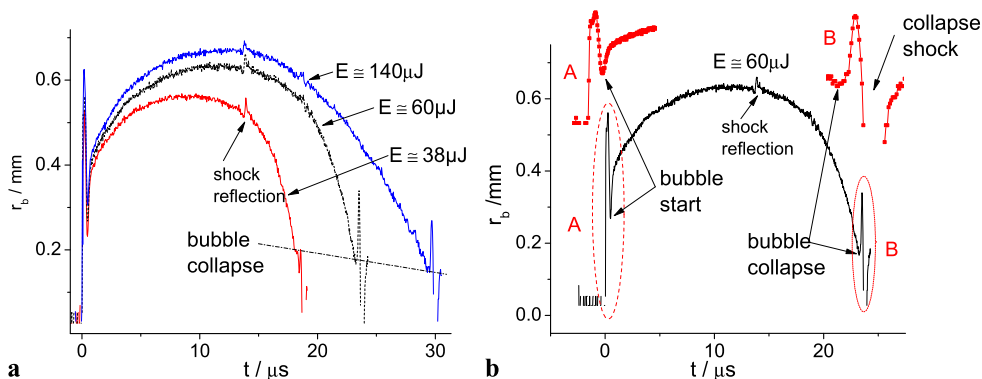


Fig. 4 Comparison of bubble radii measured in water by the introduced method (r_b , open triangles, black line as an example of bubble evolution) and CCD images (r_{ph0} , solid squares) at various time delays Δt after plasma ignition; Nd:YAG laser

Table 1 Radii of bubble size deduced from CCD images (r_{ph0}) and comparison to r_b deduced from present method at time delays Δt after plasma ignition

Δt (μs)	r_{ph0} (mm)	r_b (mm)
65	0.92	0.94
115	0.70	0.81
145	0.39	0.38
190	0.55	0.57

Fig. 5 Bubble time-distribution in water induced by a femtosecond laser: (a) for different laser energies; (b) inset for indicating the bubble initiation (A) and the first collapse (B)



20 ns and a spatial resolution of 3 μm have been obtained, which depend only on the sample rate of the oscilloscope and read out of the diode. Measurement accuracies of $U(\zeta)$ and r_0 lead to an error of r_b of $\pm 5\%$. Comparison of r_{ph0} determined from shadow images of the bubble and measured radius r_b can be realized with an error of $\pm 10\%$ (see Fig. 3).

In Fig. 5a it can be seen that the collapse radius r_c decreases with increasing laser energy E , indicated by a dashed line. However, the bubble structure at the initiation and immediately before the collapse is not exactly spherical but more or less parabolic. As a consequence, the used measuring method delivers the correct bubble start and collapse times, respectively, but the ‘bubble radius r_b ’ is an ‘equivalent radius’ to the real shadow area in the measuring plane of the bubble.

In Fig. 6, the bubble radius r_b has been measured in glycerine as a function of time with a constant temperature $T_0 = 30^\circ C$ and different initial liquid pressures $p_0 = 1$ bar (black) and $p_0 = 0.43$ bar (red). With decreasing initial liquid pressure p_0 , the bubble dimension increases as well as the collapse time t_c (time difference between maximum bubble radius and collapse). The measurements in glycerine depicted in Fig. 6, do not show collapse shocks either for $p_0 = 1$ bar or for $p_0 = 0.43$ bar.

The temperature dependence of the bubble radius is shown in Fig. 7. The initial pressure remains $p_0 = 1$ bar = const. with $T_0 = 30^\circ C$ (black curve) and $T_0 = 66^\circ C$ (red curve). Similar to Fig. 7, also both the bubble dimension r_b and the collapse time t_c increase with increasing temperature T_0 of the liquid. In contrast to Fig. 6b, now a collapse shock wave is visible due to a reduced viscosity at higher temperature (Fig. 7b, red curve).

Figure 8 shows the bubble wall velocities v_b as a function of the bubble radius r_b during the shrinking-process from the maximum bubble radius r_{max} to the minimum bubble radius r_c (collapse radius, Fig. 8a). Low Nd:YAG laser energy (7 mJ) has been used to achieve a nearly spherical bubble geometry. The results are compared to those obtained by

Fig. 6 (a) Bubble radius in glycerine as a function of time at constant temperature $T_0 = 30\text{ }^\circ\text{C}$ and various initial liquid pressures p_0 ($E_{(\text{Nd:YAG})} \approx 10\text{ mJ}$, $r_0 = 1.836\text{ mm}$); (b) time-enlarged scale of the first bubble

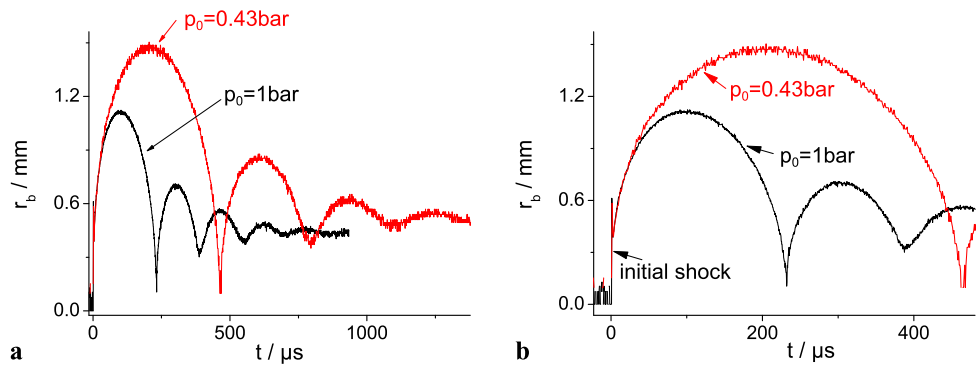


Fig. 7 Bubble radius in glycerine as a function of time for constant pressure $p_0 = 1\text{ bar}$ and different initial liquid temperatures T_0 (Nd:YAG, $r_0 = 1.863\text{ mm}$)

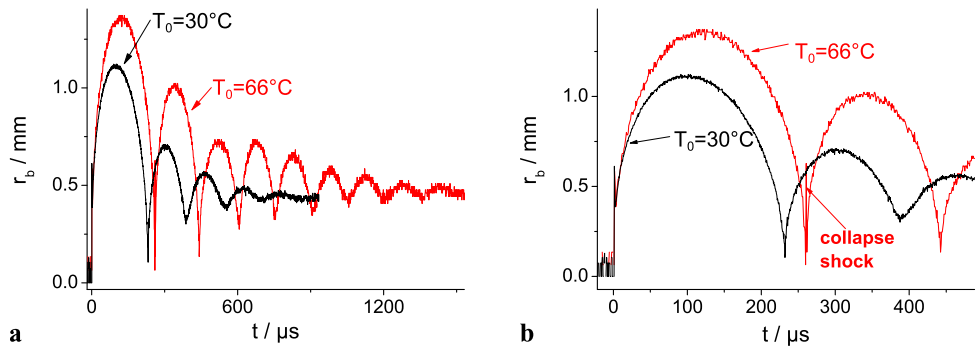
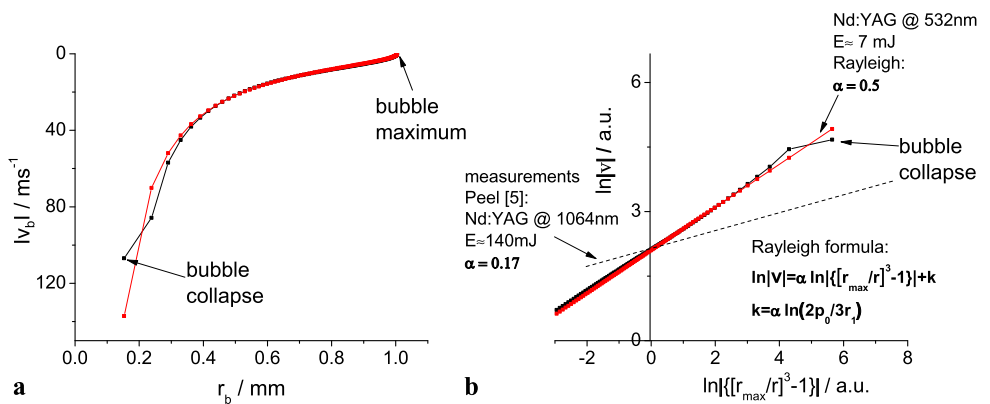


Fig. 8 Measurements of wall velocities and comparison to Rayleigh's equation in water ($E_{(\text{Nd:YAG})} \approx 7\text{ mJ}$)



Rayleigh's equation [8]:

$$v_b = \frac{2p_\infty}{3\rho_1} \left[\left(\frac{r_{\max}}{r_b} \right)^3 - 1 \right]^\alpha; \quad \alpha = 0.5 \tag{5}$$

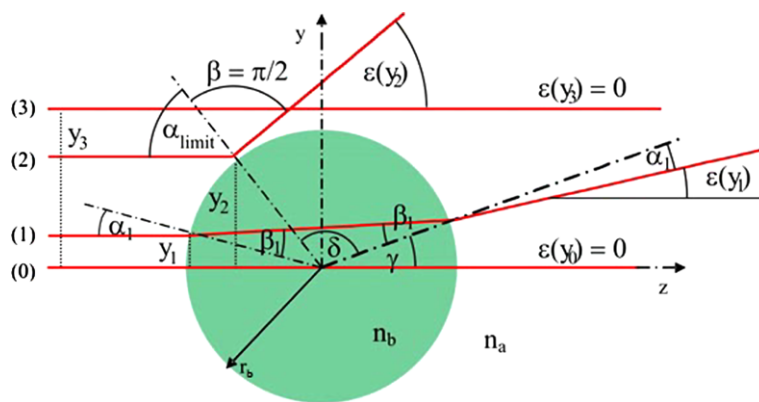
where p_∞ is the pressure in infinite liquid, ρ_1 is the liquid density, and r_{\max} is the maximum bubble radius. The first phase of the bubble shrink process shows excellent agreement, but the last phase (before collapse) is different. Experimental results for the complete bubble shrinking process could be found in the investigation of Peel et al. [5], where an exponent of $\alpha = 0.17$ was found (Fig. 8b). The discrepancy of α is due to the fact that Peel et al. [5] applied the higher laser energy in their investigation (i.e. 140 mJ) as compared to the present work (7 mJ).

A detailed investigation is beyond the scope of the present work and will be presented elsewhere [9].

5 Conclusion

A novel and powerful optical method to diagnose cavitation bubbles in liquid is presented. It allows the experimental analysis of the dynamics of laser-driven cavitation bubbles. The main advantages of bubble measurements is the high temporal and spatial resolution from the onset to the collapse of a single cavitation bubble as well as the detection of the combined shock waves generated by a single shot of a high power laser. Values of 20 ns and 3 μm , respectively, are limited by the read out system consisting of a fast photodiode and a fast oscilloscope. The error of r_b is $\pm 5\%$.

Fig. 9 Geometry of four different rays at four different distances from the optical axis: (0) on axis, (1) below angle of total reflection, (2) at total reflection, (3) ray without deflection



Although limited to spherical bubbles, CCD images during the measurements do confirm that the present method is well applicable. Especially during onset and collapse, deviation from spherical geometry was observed. However, even in that case, the bubble radius determined with the present method could be considered to be an equivalent radius.

The advantage of the novel method is its easiness to assemble, whereas the acquisition of CCD images and also the setup of the illumination are much more complicated. Furthermore, the presence of shock waves and temporal evolution of the cavitation bubble is indicated immediately.

Acknowledgement This work has been supported by the Research Committee of the University of Applied Sciences Emden/Leer.

Appendix A: Ray optics of beam deflection and estimate of diode signal

A.1 Refraction geometry

Figure 9 shows the geometry of rays of the diagnostic beam when a bubble is present. If y is not too large, e.g., $y = y_1$, the ray is refracted at both interfaces between liquid and bubble as shown in Fig. 9. The total angular change could be calculated from the following geometrical relations and from Snell’s law, respectively:

$$\alpha_1 + \beta + \gamma = \pi$$

$$\gamma = \epsilon + \alpha_1$$

$$\epsilon = 2(\beta_1 - \alpha_1)$$

$$\sin \alpha_1 = \frac{y_1}{r_b}$$

$$\frac{\sin \alpha_1}{\sin \beta_1} = \frac{n_b}{n_a}$$

As long as

$$\frac{n_a}{n_b} \frac{y_1}{r_b} \leq 1$$

refraction occurs. By means of the above six equations the angle of deflection ϵ can be calculated as

$$\epsilon(y_1, r_b) = 2 \cdot \left(\arcsin\left(\frac{n_a y_1}{n_b r_b}\right) - \arcsin\left(\frac{n_a y_1}{n_b r_b}\right) \right) \tag{6}$$

In the opposite case (ray at $y = y_2$ or at $y = y_3$), the ray is totally reflected or unaffected (see Sect. 2).

A.2 Diode signal without bubble

For an intensity profile of the diagnostic beam with a Gaussian intensity profile (see Sect. 2),

$$I(r) = I_0 \cdot e^{-2(\frac{r}{r_0})^2}$$

the power measured behind an aperture of diameter $2R$ is obtained by integrating over the aperture area, i.e.

$$P(R) = 2\pi I_0 \int_0^R e^{-2(\frac{r}{r_0})^2} r dr \tag{7}$$

For an aperture like that in the setup shown in Fig. 1, $R = r_a$ has to be inserted. This yields $P(R = r_a) = J_0$ and thus leads to Eq. (1) in Sect. 2.

A.3 Diode signal with a bubble present and the aperture positioned in infinity (i.e. $L \rightarrow \infty$)

In this case, the bubble acts like a disk. Due to deflection it blocks part of the diagnostic beam. This part could be calculated with Eq. (7) by setting $R = r_b$. In the present setup (see Fig. 1), behind the aperture, J_0 is thus reduced to $J(\zeta) = J_0 - P(R = r_b)$ which yields Eq. (2) in Sect. 2 (with $q \equiv 1$). Now, it is assumed that the diode signal, i.e. the voltage $U(\zeta)$, is proportional to $J(\zeta)$ and U_0 is the signal obtained for J_0 . Defining $u(\zeta) = U(\zeta)/U_0$, this is equal to $J(\zeta)/J_0$ and can thus be solved for r_b with Eq. (2). The result is Eq. (3) (with $q \equiv 1$).

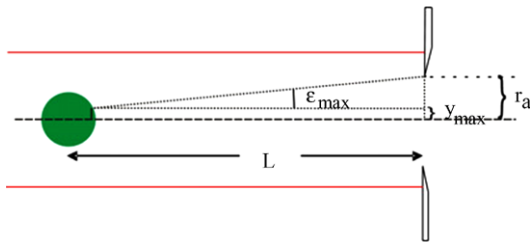


Fig. 10 Geometry of “leakage rays”

A.4 Diode signal with a bubble present and the aperture positioned at finite distance

If L is finite, rays that are only very slightly deflected may pass the aperture and thus lead to a “leakage signal” on the photodiode (see Fig. 10). As may be seen from the image observed behind the aperture (Fig. 3), in particular, this is the case for the ray on the axis and for those rays that are very close to the optical axis: The maximum value of ϵ that leaks through the aperture is obtained from $\epsilon_{\max} \approx (r_a - y_{\max})/L$ which usually is very small (because $r_a \ll L$). By inserting ϵ_{\max} into Eq. (6) (with small angle approximation of the argument) Eq. (6) may be solved for y_{\max} .

Although the bubble still blocks part of the diagnostic beam, the blocked signal consequently has to be calculated again by an integration similar to Eq. (7), but now with integration from y_{\max} to r_b (instead of integration from zero to

r_b). This leads to modifications of Eqs. (2) and Eq. (3) with a correction q that depends on ζ or r_b , respectively. The resulting q is given by Eq. (4) (one may note that $q = 1$ for L as expected for the case that the aperture is very far away).

Finally, it should be mentioned that rays at large values of y (y close to r_b) get totally reflected also at small angles ϵ and thus may leak through the aperture, too. However, as in the case above, it was verified that again, this leakage is negligible.

References

1. A. de Bosset, D. Obreschkow, P. Kobel, N. Dorsaz, M. Farhat, in *58th International Astronautical Congress* (2007). IAC-07-A2.4.04
2. O. Lindau, W. Lauterborn, AIP Conf. Proc. **524**, 385 (2000)
3. A. Vogel, S. Bush, U. Parlitz, J. Acoust. Soc. Am. **100**, 148 (1996)
4. P. Gregorcic, R. Petkovsek, J. Mozina, G. Mocnik, Appl. Phys. A **93**, 901 (2008)
5. C.S. Peel, X. Fang, S.R. Ahmad, Appl. Phys. A **103**, 1131 (2011)
6. B.P. Barber, R.A. Hiller, R.A.R. Löfstedt, S.J. Putterman, Phys. Rep. **281**, 65 (1997)
7. E.M. Englert, A. McCarn, G.A. Williams, Phys. Rev. E **83**, 046306 (2011)
8. L. Rayleigh, Philos. Mag. **34**, 94 (1917)
9. F. Hegedüs, S. Koch, W. Garen, Z. Pandula, G. Paál, U. Teubner, L. Kullmann, The effect of high viscosity on compressible and incompressible Rayleigh–Plesset-type bubble models. Int. J. Heat Fluid Flow (2012, submitted)